SAND2008-0196C

Fatigue Testing of 9 m Carbon Fiber Wind Turbine Research Blades*

Joshua Paquette†
Sandia National Laboratories‡, Albuquerque, NM, 87185

Jeroen van Dam§ and Scott Hughes§
*National Renewable Energy Laboratory**, Golden, CO, 80401*

Jay Johnson
Georgia Institute of Technology, Atlanta, GA, 30318

Fatigue testing was conducted on Carbon Experimental and Twist-Bend Experimental (CX-100 and TX-100) 9-m wind turbine research blades. The CX-100 blade was designed to investigate the use of a carbon spar cap to reduce weight and increase stiffness while being incorporated using conventional manufacturing techniques. The TX-100 blade used carbon in the outboard portion of the skin to produce twist-bend coupling to passively alleviate aerodynamic loads. In the fatigue tests, the CX-100 blade was loaded by a single hydraulic cylinder while the TX-100 blade was loaded via a hydraulically-actuated resonant loading system called the Universal Resonant Exciter. The blades were outfitted with approximately 30 strain gages as well as displacement and load sensors. Both blades survived to cycle counts sufficient to demonstrate a 20-year operational life. The CX-100 blade failed at approximately 1.6 million cycles because of a buckle and crack that formed and grew just outboard of max-chord. The TX-100 blade failed because of a crack that grew from the termination point of the spar cap at the midspan of the blade. This paper covers the results of the fatigue tests.

Nomenclature

CX	=	Carbon Experimental
TX	=	Twist-Bend Experimental
SNL	=	Sandia National Laboratories
NWTC	=	National Wind Technology Center
NREL	=	National Renewable Energy Laboratory
GEC	=	Global Energy Concepts
HP	=	High Pressure
LP	=	Low Pressure
UREX	=	Universal Resonant Exciter
IEC	=	International Electrotechnical Commission

I. Introduction

IN 2002, Sandia National Laboratories (SNL) initiated a research program[1] to demonstrate the use of carbon fiber in subscale blades[2]. From this effort, SNL created two 9-m designs with assistance from Global Energy Concepts (GEC)†† and MDZ Consulting‡‡; seven blades from each design were manufactured by TPI Composites§§. All

† Wind Energy Technology Department, MS 1124
‡ Sandia is a multiprogram laboratory operated by Sandia Corporation, a Lockheed Martin company, for the U.S. Department of Energy under contract DE-AC04-94AL85000
§ National Wind Technology Center, MS3911
** NREL is operated by Midwest Research Institute, Battelle, Contract No. DE-AC36-99-GO10337
†† Global Energy Concepts, LLC, 5729 Lakeview Drive NE, Suite 100, Kirkland, WA 98033-7340, (425) 822-9008
‡‡ MDZ Consulting, 601 Clear Lake Road, Clear Lake Shores, Texas 77565, (281) 334-5681

blades were designed for a 100 kW, constant-speed, stall-controlled turbine. The first blade set was called CX-100 (Carbon Experimental 100kW), and contained a full-length carbon spar cap, a relatively new concept at the time. The geometry of the CX-100 was based on the design of the ERS-100[3] blade at outboard span stations, but with a completely round (un-scalloped) root section. The second blade design, the TX-100 (Twist-Bend Experimental 100kW), had the same geometry as the CX-100, but featured a significantly different laminate design. The blade was designed to have passive aerodynamic load reduction by orienting unidirectional carbon plies 20° off the pitch axis in the skins from approximately 3500-mm outward. Studies[4,5,6,7,8,9] had indicated the possibility of such a method of passive aerodynamic load alleviation with material-induced twist-bend coupling; 20° was determined to be the optimum angle. Other methods of twist-bend coupling have also been suggested[10,11,12,13]. The TX-100 also contained a fiberglass spar cap that terminated at the midspan of the blade. The plan form of these blades is shown in Figure 1 with the major laminate regions shown in different colors. Visible are the carbon spar caps of the CX-100 and the carbon outboard skins of the TX-100. The unidirectional fiberglass spar cap of the TX-100 is shown in red and extends only to the midspan of the blade. It was determined that the large amount of carbon contained in the skin was adequate to carry loads outboard in this design, making a full-length spar cap unnecessary. Shear webs are represented by a black line on both drawings and were identical in dimension, placement, and layup.

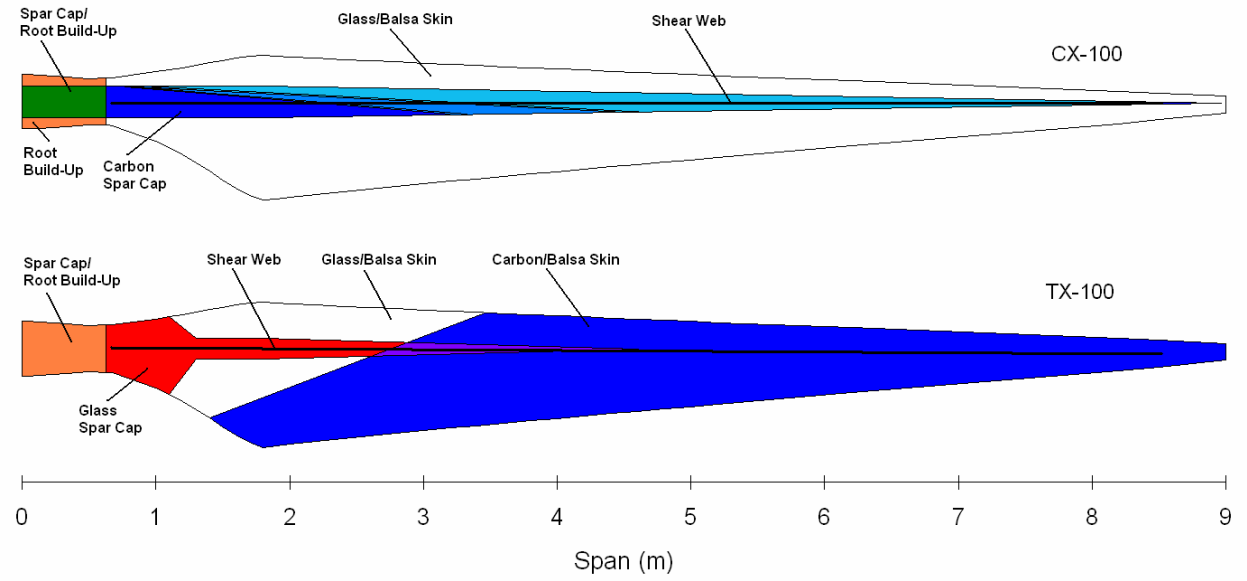

Figure 1: CX-100 (top) and TX-100 (bottom) blade plan forms and major material regions.

A suite of laboratory and field tests was proposed to verify that the manufactured blades met their design goals. In the laboratory, the blades underwent modal, static, and fatigue testing. This paper covers the results of the fatigue tests.

II. Test Setup

The CX-100 and TX-100 blades were tested in building A-60 at the National Wind Technology Center (NWTC) near Boulder, CO. This section describes the experimental setup used for both tests.

A.CX-100

A decision was made early in the test planning to load the CX-100 blade by means of a hydraulic cylinder located at the 5600-mm station of the blade. Single-point hydraulic loading has the benefit of being a simple and robust way to fatigue load a blade, but this comes at the expense of not being able to match the desired loading distribution as well as with other loading methods. An R-ratio of 0.1 on the high-pressure surface of the blade was desired as it simulates operational conditions.

§§ TPI Composites, Inc., 373 Market Street, P.O. Box 328, Warren, RI 02885, (425) 247-1050

To develop the fatigue test loading, the following fatigue-damage relationship was assumed for the materials in the blade:

$$\frac{\varepsilon}{\varepsilon_O} = A \cdot N^{-1/m} \qquad (1)$$

where ε_O is the single-cycle design fatigue strain, A is the coefficient of the ε-N curve, N is the number of loading cycles, and m is inverse slope of the ε-N curve.

The carbon spar cap of the CX-100 blade carries a majority of the flapwise bending loads and thus was the focus of the loads analysis. Figure 2 shows a comparison of thin-specimen S-N data for R=10 for infused SAERTEX/Epoxy, which makes up the CX-100 spar cap and a prepreg carbon material (Grafil/Newport)[14]. The R=10 data were used, as they produced a more conservative result than the R=0.1 data. The slopes are approximately 25 for the infused material and 45 for the prepreg material.

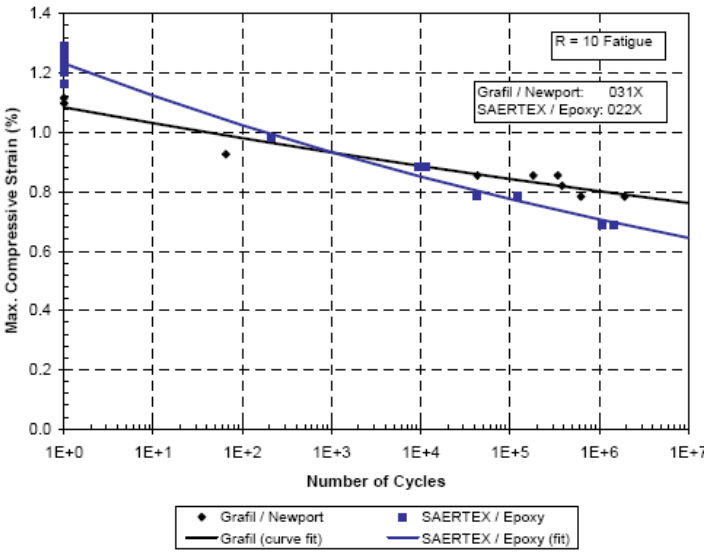

Figure 2: R=10 fatigue data for prepreg and infused (epoxy) panels (GEC).

In the fatigue calculations, a fatigue slope parameter of 12 was chosen as a compromise between the value of 10 used for glass composites and 14 used for carbon composites in the Germanischer Lloyd standards[15] as the SAERTEX fabric contains thin layers of glass between the layers of carbon. Additionally, a material safety factor of 1.63 was applied to the calculations[15]. Equation (1) along with a linear Miner's damage counting was then applied to the rainflow counts at various blade stations gathered from simulations of turbine operation performed by GEC. An example of the rainflow counts obtained at the 1800-mm station, which corresponds to the max-chord location, is shown in Figure 3. Also shown in the plot is the load for the single-cycle 50-year extreme gust event for a blade on a stall-controlled machine, for which the CX-100 was designed. This is important as it shows the difference between the fatigue and extreme loading constraints for this blade. The 50-year extreme gust load is significantly higher than the operational loads and thus drives the design.

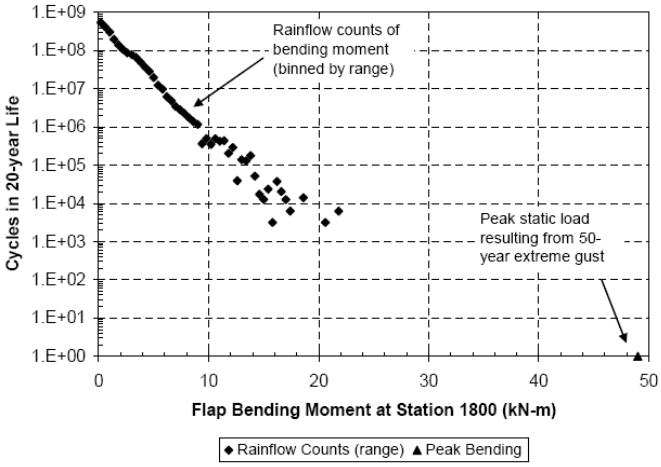

Figure 3: Comparison of CX-100 rainflow counts with peak static bending load (GEC).

There were two principal factors in the design of the fatigue test. First, the test needed to demonstrate an equivalent 20-year operation life. Second, the test needed to be completed in a reasonable cycle count (i.e. 1-4 million cycles). The fatigue calculations showed that to complete the test in a sensible test time, the target test loading would demonstrate a 20-year life in only 6,000 cycles. This test load included a test safety factor of 1.328 corresponding to IEC 61400-23[16]. Further, with the calculated load, a large amount of reserve strength would be left in the

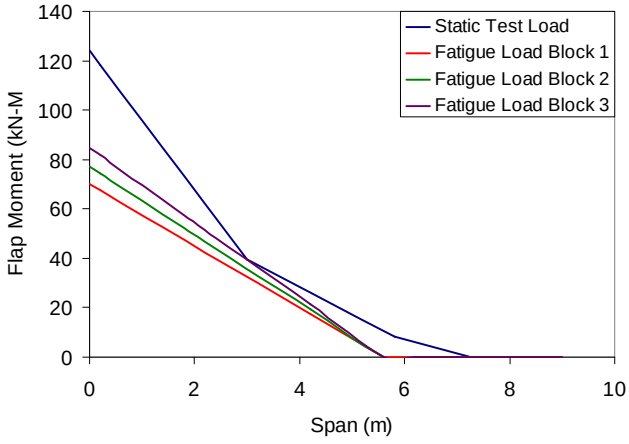

Figure 4: CX-100 fatigue test moment distributions.

examined areas. Thus it was decided that the test would begin with an initial loading of 1.25-12.5 kN at the outboard saddle, and then be increased by 10% starting at the 1 million cycle count and repeated every 0.5 million cycles thereafter. The moment distributions produced by the fatigue load targets are shown as compared to the static test load in Figure 4.

The CX-100 was conducted as a single-axis, flapwise forced displacement test. A hydraulic actuator was affixed to the blade at the 5700-m station. The actuator line-of-action was through the blade axis. A control frequency of 1.3-Hz was used to apply test loads. During the fatigue test displacement, control of the actuator was employed for test stability. Before the fatigue load blocks were performed, actuator displacement controls were determined by cycling the blade quasi-statically until the target test loads were reached. Periodically the displacement control parameters were changed to accommodate changes in blade stiffness resulting from temperature changes and damage. The actuator load is transmitted to the blade through a saddle that is composed of a steel frame and wood blade form. The blade form is constructed from laminated wood with a ½-in rubber layer between the wood and blade surface. The forced-displacement test applies a linear bending moment from the blade root to the loading station; the baseline applied bending moment and target test bending moment are shown in Figure 4. The applied bending moment was designed to match the target test load at the fatigue-critical span of 2-4 m, which corresponds to spans from the maximum chord station to near the midspan of the blade.

The CX-100 blade was outfitted with several data acquisition and structural health monitoring systems. The baseline data acquisition system used to monitor the test was composed of 28 strain gages. The locations of the strain gages, are shown in Figure 6. Strain, load, and displacement were monitored and recorded for the duration of the test as peak-valley pairs.

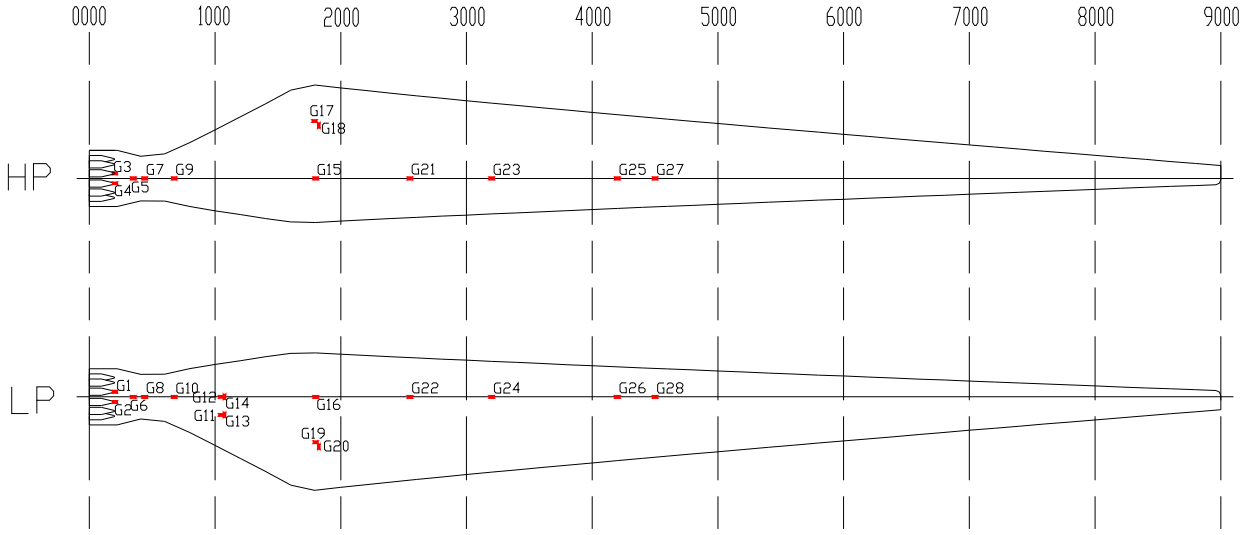

Figure 6: CX-100 fatigue test strain gage layout.

B. TX-100

The fatigue load for the TX-100 blade was analyzed similarly to that of the CX-100 blade, originating from Equation (1). However, a slope coefficient of 12 was used instead of 14, as in the previous analysis, to account for the flap loads being oriented at 20° from the carbon fiber direction. In addition, the blade was to be loaded via a resonant loading method that allowed the target loading to be better approximated along the blade span and did not restrict the twist dynamics of the blade. Like for the CX-100, rainflow counts of load cycles acquired from system dynamics simulations were used to compute 20-year damage fractions. The cycle counts from the max-chord station are shown in Figure 6. For the TX-100 blade, the 50-year gust load was removed from design consideration, as this caused

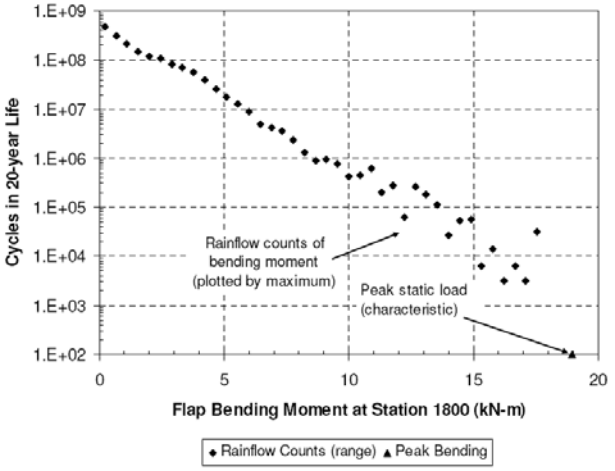

Figure 5: Rainflow counts at 1800 mm station of TX-100 blade (GEC).

the design to not have the desired amount twist-bend coupling. This was seen as a reasonable design envelope modification[17] because the blades were intended for research use only, and the aforementioned load case is not typically important for modern pitch-controlled turbines. The removal of the 50-year extreme parked load case resulted in an extreme single-cycle load, significantly closer to the fatigue load range than the CX-100 test (see Figure 3).

Test loading targets were developed from the damage analysis. Similar to the CX-100 test, the loads were partially driven by the desire for a test of reasonable duration. Also like the CX-100, it was decided that the load would be increased in increments of 10% every 0.5 million cycles starting at the 1 million cycle count. To serve as a guide, fatigue test loading distribution for 1, 2, and 4 million cycle tests were developed. These load distributions are shown in Figure 7, along with the moment distribution from an earlier static test of another TX-100 blade. The load step increase schedule would show a 20-year life at the 2 million cycle count.

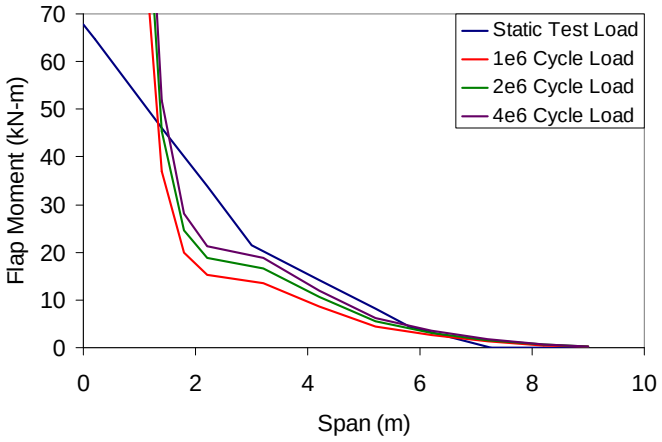

Figure 7: TX-100 fatigue peak loading targets for one, two, and four million cycle tests.

A resonant test apparatus[18] was used to conduct the TX-100 fatigue test. The test was configured as a single-axis flapwise resonant test, which was conducted by affixing a resonant mass and ballast saddles to the cantilevered test article. Hydraulic actuators controlled the resonant mass. By exciting the resonant mass at the natural frequency of the system, an alternating test bending moment was applied to the blade. The location and weight of the excitation mass and ballast saddles prescribed both the mean load and the characteristic shape (mode shape) of the alternating moment. The weight and actuated distance of the resonant mass controlled the amplitude of the alternating test load.

The resonant test setup had several advantages over a forced-displacement test, especially for this bend-twist coupled blade, because the resonant test method did not artificially impart a torque to the test article, and thus did not constrain the natural bend-twist coupling of the TX-100 blade. Employing a forced displacement test, as was done for the CX-100 test, would have artificially attenuated the bend-twist coupling of the blade. For forced-displacement testing, as the blade is displaced out–of-plane, the effective chordwise load application line-of-action changes and imparts an undesirable torque to the blade. In addition, resonant testing allowed for better matching of the target test bending moment over the length of the blade caused by the characteristic shape of the alternating load, in comparison to the linear bending moment applied by a forced-displacement test.

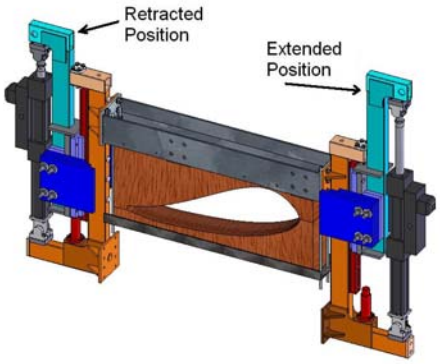

Figure 8: UREX Schematic.

A novel resonant test apparatus was developed at NREL for this test. The UREX (Universal Resonant EXciter) was used to apply the test loading. The UREX was developed specifically for the unique aspects of testing bend-twist coupled blades. The UREX uses a pair of hydraulic actuators mounted to the blade through a ballast saddle. The actuators are located on each side of the blade (see Figure 8). This sidesaddle arrangement has advantages over previous single-actuator designs. The primary advantage of the UREX is that the rotational inertia is minimized in comparison to mounting the actuator and resonant mass above the center of the blade, which could impart undesired torsional loading, thus distorting the bend-twist response of the test article. Figure 9

Figure 9: TX-100 Test setup photograph.

provides a photograph of the TX-100 test setup. In addition, although not employed for the TX-100 test, the UREX can tune an applied torsional loading by adjusting the displacements, relative phases, and associated oscillating masses for the two independent actuators.

Locations and ballast masses were optimized by using resonant test codes developed at NREL to apply a test bending moment to match the target test load and maintain the r-ratio of R=0.1. The UREX system was located at the 1600-mm station, with a ballast saddle at the 6750-mm station. The UREX system and ballast saddles were located in spanwise areas away from critical structural regions of the blade. This positioning was in an effort to minimize the potential artificial stiffening of the loading station, and to allow for a natural bend-twist degree of freedom. The load imparted by the UREX onto the TX-100 blade for the initial load step is shown in Figure 10 as compared to the target test loading and the test load from a previous static test.

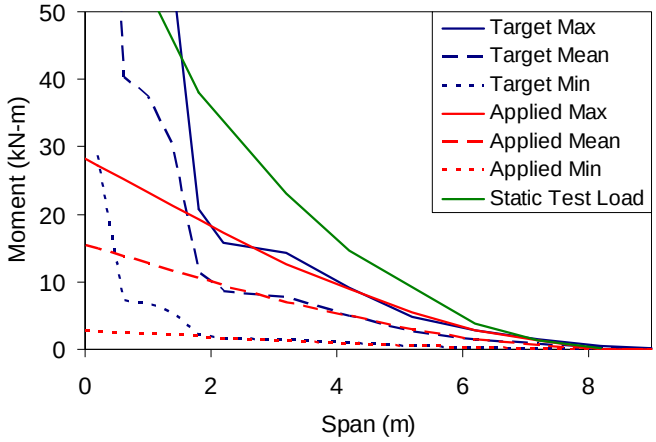

Figure 10: Calculated UREX fit of 4 million cycle target load for TX-100 fatigue test.

The TX-100 blade was outfitted with several data acquisition and structural health monitoring systems. The baseline data acquisition system used to monitor the test was composed of 30-strain gages. The locations of the strain gages, which will be referenced later, are shown in Figure 11. Strain, load, and displacement were monitored and recorded for the duration of the test as peak-valley pairs.

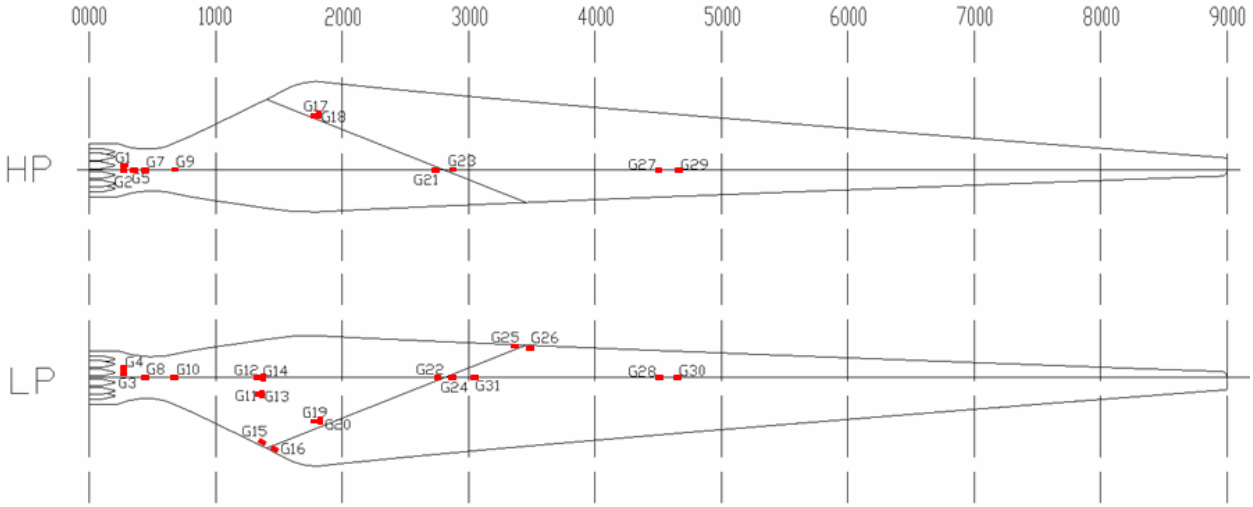

Figure 11: TX-100 fatigue test strain gage layout.

III. Test Results and Analysis

After each test, the data were analyzed and a postmortem inspection was performed on the blades. The data were reduced by block averaging data points, 1000 points per block. The general strategy was to look at measures of overall damage compared to local areas.

A.CX-100

Assessing a measure of global damage gives insight into how degradation, which is most often a local phenomenon, shows up at the level of the overall structure. Global measures of damage in wind turbine blades include, but are not limited to tip displacements and lower order modal frequencies and shapes. Local measures of damage come in the form of individual sensors placed in locations very near to damage and in the higher order mode shapes and frequencies.

The global stiffness can be measured by the following:

$$K = \frac{P_{max} - P_{min}}{d_{max} - d_{min}} \qquad (2)$$

where K is a global stiffness measure, P_{max} and P_{min} are the maximum and minimum load levels for an individual cycle, and d_{min} and d_{max} are the corresponding maximum and minimum displacements for the cycle.

The global stiffness of the CX-100 blade during the fatigue test is shown in Figure 12. The data is normalized by the initial value. Evident in the plot is softening beginning around 1.0 million cycles. The total amount of stiffness degradation was approximately 10% at the end of the test.

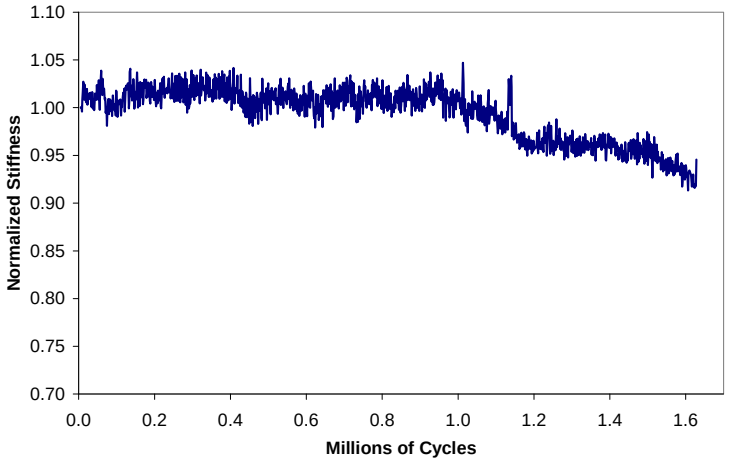

Figure 12: Normalized stiffness at saddle for CX-100 fatigue test.

The results from the strain gages can be analyzed in a similar way, substituting strain for deflection in Equation (2). This gives an indication of how the structure is changing at a point location. It should be noted that this does not necessarily indicate the stiffness changes as these results can be effected by changes in the principle strain directions at a point and other load path changes. Nonetheless, the results are useful as they point to changes occurring in the blade resulting from fatigue damage. Results from strain gages located in the aft panel region near max-chord (see Figure 6) are shown in Figure 13. Gages 19 and 20 show a marked change beginning shortly after 1.25 million cycles. The change in these measurements is seen to be up to 30%.

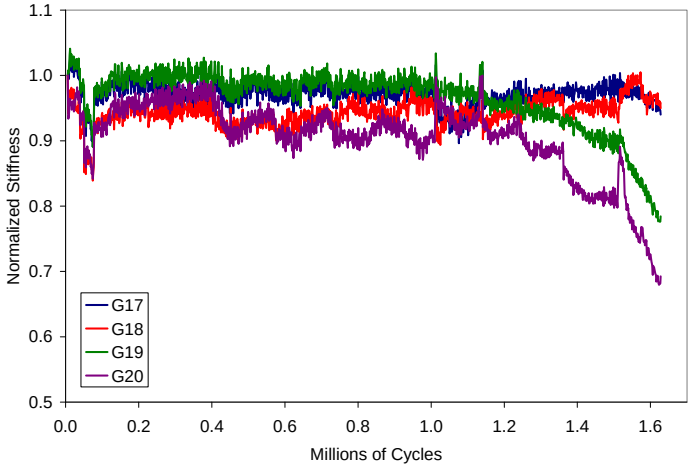

Figure 13: Normalized stiffness at CX-100 strain gages 17, 18, 19, and 20.

Figure 14 shows the results from the strain gages located on the spar cap from 25% to 50% of the blade span. These strain gages display more dramatic changes beginning at about 1.1 million cycles. Increases in local stiffness can be attributed to changes in load path.

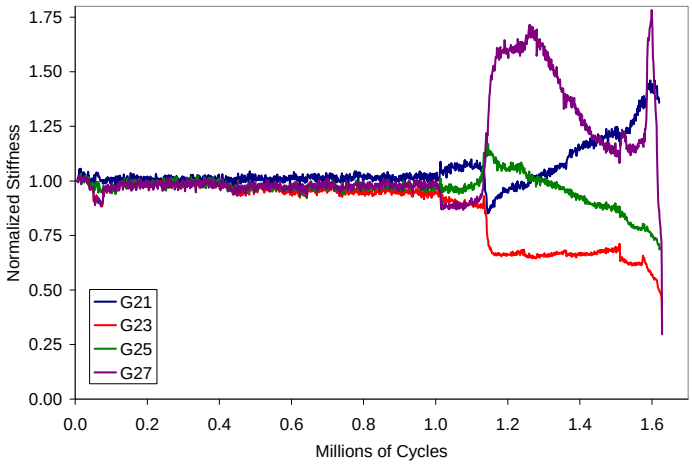

Figure 14: Normalized stiffness at CX-100 strain gages 21, 23, 25, and 27.

The CX-100 test proceeded without significant damage until the 1.5-million cycle count. Throughout the test, a notable dimple in the blade was apparent in the low-pressure skin, at the 1100-mm station toward the trailing edge of the blade. The out-of-plane depth of the dimple progressed during testing. Spanwise surface cracks were noted at the 1.5-million cycle count between the 1200-mm and 1400-mm stations. These surface cracks formed at the junction of the carbon spar cap and the trailing edge panel. By the 1.6-million cycle level, the cracks had progressed through the thickness of the skin and the test was stopped. The out-of-plane movement of the skin once the crack had fully penetrated the skin became progressively larger. In addition, the blade stiffness had decreased by approximately 12% from the initial stiffness, and the lead-lag motion of the blade progressively

increased. Subsequent investigations indicate the increased crack length and development of a disbonding between the LP skin and spar cap led to increasing larger out of plane panel deformation leading to gross panel buckling. Figure 15 provides a photograph of the damage area of the CX-100.

Figure 16: CX-100 low-pressure skin damage area.

B. TX-100

The global stiffness of the TX-100 blade was measured with a different method because displacement data from a load application point were unavailable. Multiple sensors were mounted on this blade as the TX-100 served as a test bed for structural health monitoring sensors[19]. Among the health monitoring sensors were several accelerometers at the blade tip which were used by a team from Purdue University[20]. Double-integrating the response from tip accelerometer provided test displacements. Using these displacements along with the moment from root-mounted strain gages, and then inputting the results into Equation (2) provided the stiffness of the blade measured at the tip. The results are shown in Figure 16.

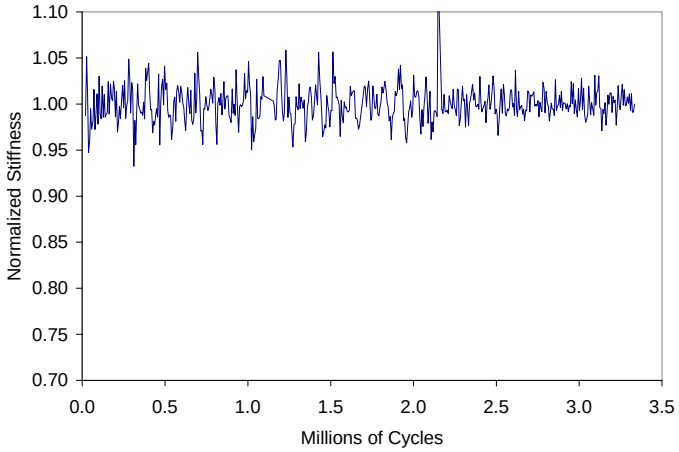

Figure 15: Normalized stiffness at blade tip for TX-100 fatigue test.

The strain gage results can be examined to look for signs of damage occurring earlier than what might be seen in the aggregated data taken at the tip. Figure 17 provides the response from a strain gage mounted just outboard of the tip of the glass spar cap (see Figure 11). The gage shows that this area began to experience softening before 1 million cycles and gradually progressed throughout the test.

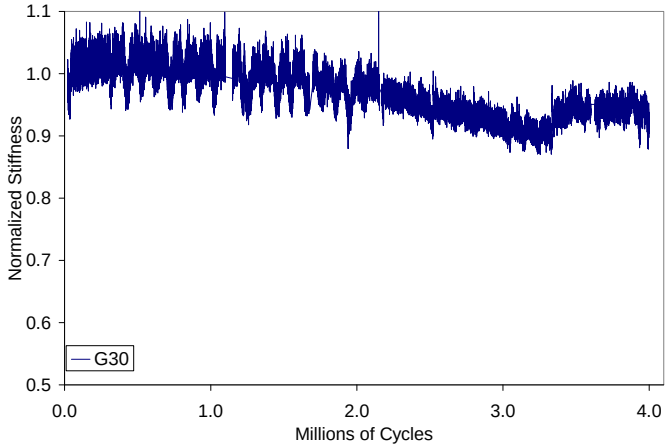

Figure 17: Normalized stiffness of TX-100 at strain gage 30.

Damage to the TX-100 manifested itself as fine gel-coat cracks on the high-pressure side of the blade, running at an angle of 65° with respect to the spanwise axis of the blade. These cracks occurred throughout much of the span of the blade, but were most apparent in the 4000-mm to 5600-mm span of the blade. The 65-degree angle coincides with the principal axis of the ±45-degree fiberglass laminate. These gel-coat cracks progressed in length and gap width from the 723k cycle count to the 2.4-million cycle count until out-of-plane movement of the skins abutting the crack was apparent. The length and gap of the crack increased, and the principal axis of the crack front deviated from 65 degrees to 20 degrees, which is the same as the principal direction of the carbon fiber laminate. Once the principal direction of the crack coalesced to the principal direction of the carbon fiber, the crack-length rate and out-of-plane distortion became progressively larger. The test was stopped at the 4-million cycle count because of excessive torsional motion of the blade tip and an accelerated increase in rate of crack length. Figure 18 provides a photograph of the damaged area on the high-pressure surface of the blade at the 4500-mm station; the gel coat was removed to expose the fiberglass and carbon fiber laminate. The incipient cause of damage to the TX-100 was the outboard

termination of the spar cap, which ends at the 4500-mm station. The spar cap termination caused a stress riser in the stressed-skin laminate.

Figure 18: TX-100 high-pressure skin damage area.

IV. Conclusion

Both the CX-100 and TX-100 blades demonstrated 20-year equivalent fatigue test loads. The CX-100 needed to complete only 6,000 cycles at its initial load level to demonstrate adequate fatigue resistance but survived past 1.6 million cycles. The TX-100 design was a less stiff design and needed to survive to 2.0 million cycles under the load step regime discussed. The blade failed at over 4 million cycles. While further validation of the blade designs through field testing is planned, the laboratory tests provide a favorable result for hybrid glass/carbon designs. The CX-100 incurred incipient damage above the target fatigue test load. The epicenter of the damage was the interface of the carbon spar cap and the glass/balsa panels, an interface between two laminates with greatly differing stiffness. The TX-100 also maintained structural integrity (stiffness) past the design fatigue life but grew a severe crack along the carbon fiber line beginning at the sharp termination of the spar cap. Thus, while both blades withstood the required number of cycles to demonstrate a 20-year operational life, the unique design aspects of both blades played a role in their eventual failure. Also of importance was that while the fatigue calculations were based on fiber direction material properties, the off direction material properties played a role in the eventual failure of both blades. This demonstrates the difficulty in incorporating innovative design features in a fatigue sensitive structure as well as the difficulty of performing accurate fatigue life predictions based on limited material property data and simple models.

Acknowledgments

The U.S. Department of Energy is thanked for the support of blade development programs and structural testing. Special thanks go to Mike Jenks of NREL who was instrumental in the setup and test conduction, and Dayton Griffin and Tim McCoy of GEC who performed the fatigue test load calculations. The authors would like to acknowledge Mark Rumsey, Perry Jones, and Wesley Johnson of SNL; Jason Cotrell and Dave Simms of NREL; Derek Berry of TPI Composites, Inc., Alan Beattie of PAC; and Mike Zuteck of MDZ Consulting for their assistance in the preparation and performance of these tests.

References

1 Ashwill, T. and Laird, D., "Concepts to Facilitate Very Large Blades," Proceedings, ASME/AIAA Wind Energy Symposium, Reno, NV, 2007.

2 Ong, C.-H. and Tsai, S. W., "The Use of Carbon Fibers in Wind Turbine Blade Design: A SERI-8 Blade Example," SAND2000-0478, Sandia National Laboratories Contractor Report, March 2000.

3 TPI Composites, Inc. Final Project Report, "Blade Manufacturing Improvements Development of the ERS-100 Blade," SAND2001-1381, May 2001.

4 Veers, P. S., Bir , G., and Lobitz D. W., "Aeroelastic Tailoring in Wind-Turbine Blade Applications," Proceedings, Windpower '98 Meeting, pp. 291-304.

5 Lobitz, D. and Veers, P., "Aeroelastic Behavior of Twist-coupled HAWT Blades," ASME/AIAA Wind Energy Symposium, Reno, NV, 1998, pp. 75-83.

6 Lobitz, D. and Laino, D., "Load Mitigation with Twist-coupled HAWT Blades," ASME/AIAA Wind Energy Symposium, Reno, NV, 1999, pp. 124-134.

7 Lobitz, D., Veers, P. S., and Laino, D. J., "Performance of Twist-Coupled Blades on Variable Speed Rotors," Proceedings, ASME/AIAA Wind Energy Symposium, Reno, NV, 2000, pp. 404-412.

8 Lobitz, D. W. Veers, P. S., Eisler, G. R., Laino, D. J.,Migliore, P. G., and Bir, G., "The Use of Twist-Coupled Blades to Enhance the Performance of Horizontal Axis Wind Turbines," SAND2001-1303, May 2001.

9 D. Griffin, "Evaluation of Design Concepts for Adaptive Wind Turbine Blades," SAND2002-2424, Sandia National Laboratories Contractor Report, August 2002.

10 Ong, C.-H. and Tsai, S. W., "Design, Manufacture and Testing of a Bend-Twist D-spar," Sandia National Laboratories Contractor Report, SAND99-1324, June 1999.

11 Wetzel, K. and Locke, J., "Uncoupled and Twist-Bend Coupled Carbon-glass Blades for the LIST Turbine," Proceedings, ASME/AIAA Wind Energy Symposium, Reno, NV, 2004, pp. 13-23.

12 Locke, J. and Valencia, J., "Design Studies for Twist-Coupled Wind Turbine Blades," SAND2004-0522, Sandia National Laboratories, Albuquerque, NM, June 2004.

13 Wetzel, K., "Utility Scale Twist-Flap Coupled Blade Design," Proceedings, ASME/AIAA Wind Energy Symposium, Reno, NV, 2005, pp. 382-394.

14 Griffin, D., "Alternative Materials for Megawatt- Scale Wind Turbine Blades: Coupon and Subscale Testing of Carbon Fiber Composites", 44th AIAA Aerospace Sciences Meeting and Exhibit, Reno, NV, 2006.

15 Germanischer Lloyd (1999). Rules and Regulations IV – Non-Marine Technology, Part 1 – Wind Energy, Regulation for the Certification of Wind Energy Conversion Systems.

16 International Electrotechnical Commission. (1999). IEC 61400-1: Wind turbine generator systems – Part 1: Safety Requirements, 2nd Edition. International Standard 1400-1.

17 Berry, D., "Design of 9-meter Carbon-Fiberglass Prototype Blades Final Project Report," SAND Report in preparation, Sandia National Laboratories, Albuquerque, NM, 2008

18 White D., Musial, W., Engberg, S. "Evaluation of the New B-REX Fatigue Testing System for Mult-Megawatt Wind Turbine Blades" Proceeding, ASME/AIAA Wind Energy Symposium, Reno, NV, 2005

19 Rumsey, M. and Paquette J., "Experimental Results of Structural Health Monitoring of Wind Turbine Blades," 46th AIAA Aerospace Sciences Meeting and Exhibit, Reno, NV, 2008.

20 Adams, D.; White, J.; Rumsey, M.; van Dam, J., "Impact, Loading and Damage Detection in Carbon Composite TX-100 Wind Turbine Rotor Blade," *46th AIAA Aerospace Sciences Meeting and Exhibit*, Reno, NV, 2008.